Fabrication of BiOI Nanoflowers Decorated TiO₂ Nanotube Arrays on Porous Titanium with Enhanced Photocatalytic Performance for Rhodamine B Degradation

Yu-Long Xie[*]*, Li-Fang Guo, Cuo-Ji Ben*

Key Laboratory of Resource Chemistry and Eco-environmental Protection in Tibetan Plateau of State Ethnic Affairs Commission, School of Chemistry and Chemical Engineering, Qinghai Minzu University, Xining, Qinghai, 810007, China
[*]E-mail: yulongxie2012@126.com

We successfully deposited the BiOI nanosheets onto the surface of three-dimensional porous TiO₂ nanotube arrays (NTs) substrate by the successive ionic layer adsorption and reaction (SILAR) method. The coupling of BiOI and TiO₂ NTs significantly improved the photocatalytic activity of Rhodamine B (RhB) degradation under visible-light irradiation. By further investigating the charge transportation and separation behaviors, the energy band structure experiments were carried out. Thus, a possible photocatalysis mechanism of p-n Heterojunction was proposed, which not only facilitated the effective separation of photoelectrons, but also proved the advanced capability of photoelectrocatalysis in the degradation of organic dyes. According to the results of calculation and experiment, the possible mechanism of enhancement of photocatalytic activity of BiOI/TiO₂ NTs was proposed, and the conclusion was confirmed by the photocurrent experiment.

1. INTRODUCTION

Over the past decades, photocatalysis has attracted increasing interest in energy and environmental applications [1, 2]. Semiconductor photocatalysts have excellent photocatalytic (and/or electrochemical) activity and are considered as ideal materials for solving energy and environmental problems [3-7]. Over the past several years, TiO₂ has achieved more attention due to its biological and chemical inertness, acid resistance, non-toxicity, favorable band edge positions, and long-term stability [8-11]. TiO₂ nanosheets with various morphologies were investigated to improve the electro-chemical performance. Although, TiO₂ is a very good photocatalsyts, it could not be effectively utilized under

visible light since it is only absorbs ultraviolet light no longer than 387.5 nm because of the band gap of 3.2 eV, which only occupies about 4% of sunlight [12]. In order to improve their photocatalytic performances, a large number of coupled semiconductors [13-24], such as SiO_2/TiO_2, CdS/TiO_2, ZnO/TiO_2, SnO_2/TiO_2, ZrO_2/TiO_2, $BiVO_4/TiO_2$, $BiOI/TiO_2$, $BiOI/NiO$, $BiOCl/BiOI$, $Pd/BiOCl/BiOI$, $BiVO_4/BiOI$, and $CdS/WO_3/BiOI$ composites have been fabricated and they showed higher photocatalytic performances than their pristine forms.

In this respect, the bismuth oxyiodide (BiOI) is one of the new materials that have been recognized as a visible-light driven photocatalyst for this application because of its narrow energy band gap (1.7-1.9 eV) and its chemical stability [25-27]. However, because of the fast rate of charge recombination and poor conductivity of BiOI, the ability of photocatalytic degradation of phenol is low [28, 29]. In order to improve the electron transfer performance of BiOI, many methods have been studied, such as structure design, doping and heterojunction [30-33]. Fortunately, coupling BiOI with TiO_2 exhibit better charge separation and attractive photocatalytic performance [34-41] on the degradation of organic pollutants under visible-light irradiation.

Compared with TiO_2 powders, TiO_2 nanotube arrays (TiO_2 NTs) have highly ordered tubular structure and high specific surface area prepared on titanium substrate [42], which showed better photocatalytic and photoelectronic properties. Dai et al. [43] reported $BiOI/TiO_2$ NTs p-n junction, and the $BiOI/TiO_2$ NTs samples exhibited the high visible light absorption, photocurrent response and significantly enhanced photoelectrocatalytic activity for the degradation of MO dyes. Liu et al. [7] reported TiO_2 NTs decorated with BiOI as an enhanced photocatalyst for degradation of organic pollutants under visible-light irradiation. Liu et al. [44] reported $BiOI/TiO_2$ NTs p–n heterojunctions by loading BiOI nanoflakes on TiO_2 NTs walls, and the $BiOI/TiO_2$ NTs samples showed the high visible-light photocurrent response and photoelectrocatalytic activity. Therefore, the effective electron transportation along the vertical walls of TiO_2 NTs would significantly reduce the recombination of electron/hole pairs in BiOI.

Considering the high specific surface area, in this study, the three-dimensional porous TiO_2 NTs were prepared in porous titanium substrate by a simple anodization method. BiOI nanosheets were deposited onto the surface of the three-dimensional porous TiO_2 NTs by the successive ionic layer adsorption and reaction (SILAR) method. The three-dimensional porous $BiOI/TiO_2$ NTs photoelectrode exhibited superior photocatalytic and photoelectronic performances. The simple synthesis and high photoelectric activity of three-dimensional porous $BiOI/TiO_2$ NTs would provide the template for the preparation and application. And the results showed that the three-dimensional porous $BiOI/TiO_2$ NTs nanocomposite exhibited more efficient photocatalytic activity than pure TiO_2 NTs.

2. EXPERIMENTAL

The three-dimensional porous TiO_2 NTs were prepared by anodization of porous titanium sintered plate of 1000 μm thickness in a two-electrode cell of 0.3 wt% NH_4F and 2.0 vol.% H_2O in ethylene glycol at 60 V. BiOI nanosheets were deposited on the surface of TiO_2 NTs by the SILAR method. Initially, the three-dimensional porous TiO_2 NTs samples were immersed in 3 mmol·L^{-1}

$Bi(NO_3)_3 \cdot 5H_2O$ solution for 30 s. Then, the samples were cleaned with deionized water, and were immersed in 3 mmol$\cdot$L^{-1} KI solution for 1 min, and cleaned again with deionized water. This step was repeated for several cycles to prepare BiOI/TiO$_2$ NTs nanocomposites. The samples prepared with 3, 7 and 12 cycles were marked as BiOI/TiO$_2$ NTs-3, BiOI/TiO$_2$ NTs-7, BiOI/TiO$_2$ NTs-12. Finally, prepared BiOI/TiO$_2$ NTs nanocomposites were calcined for 2 h at 300 °C in air.

The electrochemical properties of BiOI/TiO$_2$ NTs nanocomposites were investigated in 0.5 M Na$_2$SO$_4$ solution using a typical three-electrode system with the CHI 660E electrochemical workstation at room temperature. The prepared samples was served as the working electrode, and Ag/AgCl and Pt mesh served as the reference and counter electrodes, respectively. The samples were illuminated with a solar simulator equipped with a 500 W Xe lamp (CELS500). The dye concentration was determined with a UV-VIS-NIR spectrophotometer UV-3600 Plus, SHIMADZU) by detecting the maximum absorption wavelengths for RhB at 552 nm.

X-ray diffraction (XRD) patterns of samples were recorded using a diffractometer (Vltima Ⅳ, Rigaku). The morphologies of samples were examined by a field emission scanning microscope (FE-SEM, Sigma 500, Carl Zeiss, Germany). The optical absorption properties of the samples were investigated by a UV-VIS-NIR spectrophotometer (UV-3600 Plus, SHIMADZU) using BaSO$_4$ as the reference. The samples were illuminated with a solar simulator equipped with a 150 W Xe lamp (Tungsten). The dye concentration was determined with a UV-VIS-NIR spectrophotometer UV-3600 Plus, SHIMADZU) by detecting the maximum absorption wavelengths for RhB at 552 nm.

3. RESULTS AND DISCUSSION

Fig. 1 shows the FE-SEM images of the porous titanium sintered plate, pure three-dimensional porous TiO$_2$ NTs, and the three-dimensional porous BiOI/TiO$_2$ NTs-7 samples. Fig. 1(a) image clearly shows the porous titanium sintered plate. We can see that the porous titanium is made up of a large number of titanium particles. At the same time, the porous titanium sintered plate has many pores. Fig. 1(b) shows the morphology of the pure three-dimensional porous uniform arrays of TiO$_2$ NTs of the porous Ti substrates. Fig. 1(c) and (d) shows the morphology and microstructure of the three-dimensional porous BiOI/TiO$_2$ NTs-7 nanocomposites after the deposited BiOI nanosheets on the surface of TiO$_2$ NTs by the SILAR method. As shown in Fig. 1(c) and (d), BiOI nanosheets with the thickness of 10 nm were covered on the surface by the SILAR, and the thin BiOI nanosheets assembled to form nanoflowers.
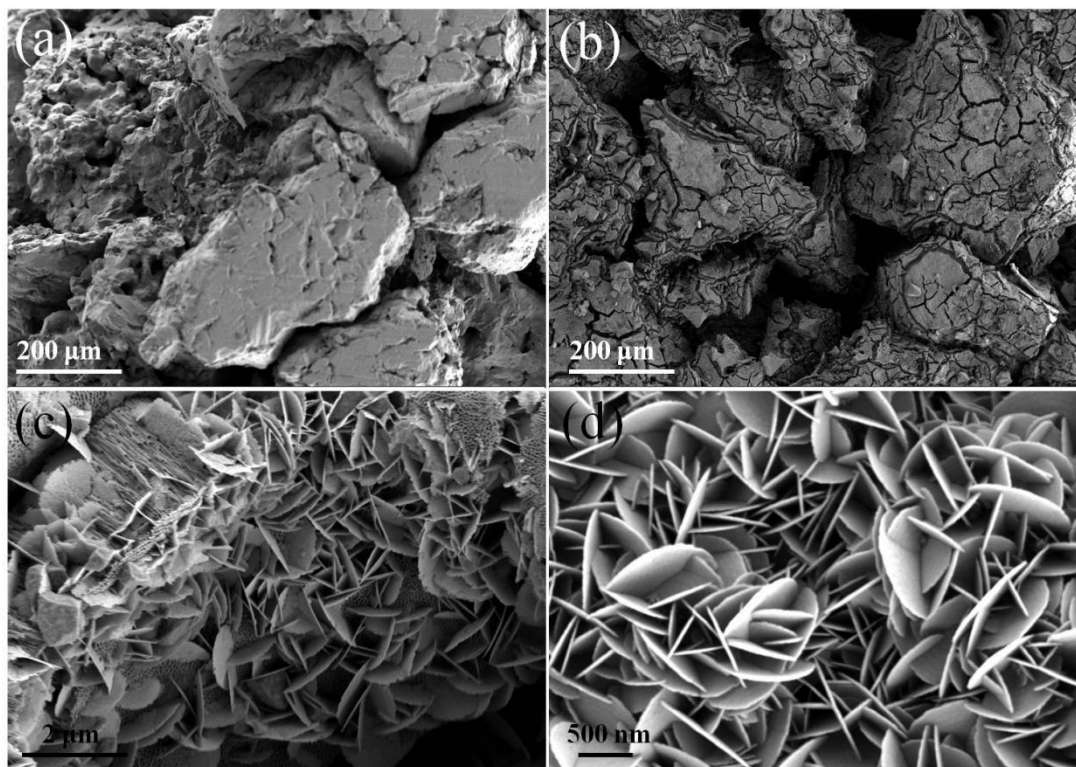
Figure 1. (a) SEM image of porous Titanium sintered plate, (b) SEM image of three-dimensional porous TiO$_2$ NTs, (c) and (d) SEM images of three-dimensional porous BiOI/TiO$_2$ NTs-7.

We further confirmed the X-ray powder diffraction (XRD) studies of the product (Fig. 2). The X-ray powder diffraction analysis showed that the as-prepared powders were a mixture phase of BiOI, anatase TiO$_2$, and Ti. The three-dimensional porous BiOI/TiO$_2$ NTs-7 samples displayed diffraction peaks, which could be indexed to the characteristic peaks of BiOI (JCPDS file no. 10-0445), the additional peaks are identified as the anatase form. After deposition of BiOI on TiO$_2$ NTs, the new peaks are observed in addition to the diffraction peaks from the TiO$_2$ NTs.

In order to provide a reasonable interpretation for the improved photocatalytic activity of three-dimensional porous BiOI/TiO$_2$ NTs heterostructure photocatalysts, photoelectrochemistry performances of TiO$_2$ NTs, BiOI/TiO$_2$ NTs-3, BiOI/TiO$_2$ NTs-7, and BiOI/TiO$_2$ NTs-12 heterostructure as photoanodes were investigated. Fig. 3 shows the transfer and recombination rate of the photoexcited electrons and holes by the photocurrent response.
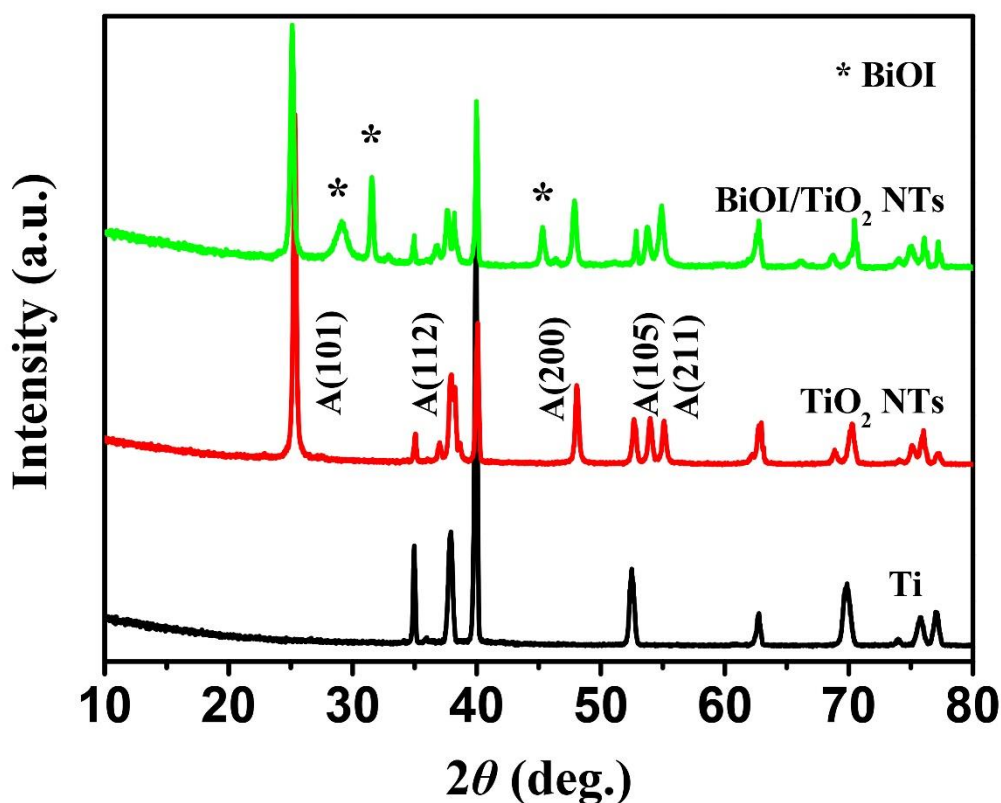
Figure 2. XRD patterns of porous Ti, TiO$_2$ NTs, and BiOI/TiO$_2$ NTs-7.

It is obvious that the three-dimensional porous BiOI/TiO$_2$ NTs composites shows higher photocurrent compared with pure TiO$_2$ NTs under visible light irradiation, and BiOI/TiO$_2$ NTs-7 evidently demonstrates the highest photocurrent density. It represents that the formation of BiOI/TiO$_2$ NTs heterojunction improves the separation efficiency of photogenerated charge carriers, leading to the promoted photocatalytic activity. As we can see clearly from the Fig. 3, the BiOI/TiO$_2$ NTs prepared by SILAR method resulted in the increase of the photocurrent. Higher photocurrent of BiOI/TiO$_2$ NTs sample may be due to presence of BiOI in the composites, and make these composites more photoactive under visible light. It could be seen clearly that the BiOI/TiO$_2$ NTs-7 showed the highest efficiency of photoelectric transformation. However, with the increasement of BiOI deposition cycles, BiOI/TiO$_2$ NTs-12 showed low photocurrent response. The reason could be attributed that the visible light was reflected at the surface of too much BiOI nanosheets layer on top of the coaxial BiOI/TiO$_2$ NTs in BiOI/TiO$_2$ NTs-12 sample, but the coaxial BiOI/TiO$_2$ NTs microstructures could achieve multiple reflections. Therefore, the high visible light response of BiOI/TiO$_2$ NTs-7 with coaxial BiOI/TiO$_2$ NTs structures displayed the high photoelectric conversion efficiency, which would be attributed to the foundations for the photoelectric conversion and significantly enhanced photoelectrocatalytic degradation of organic pollutants.
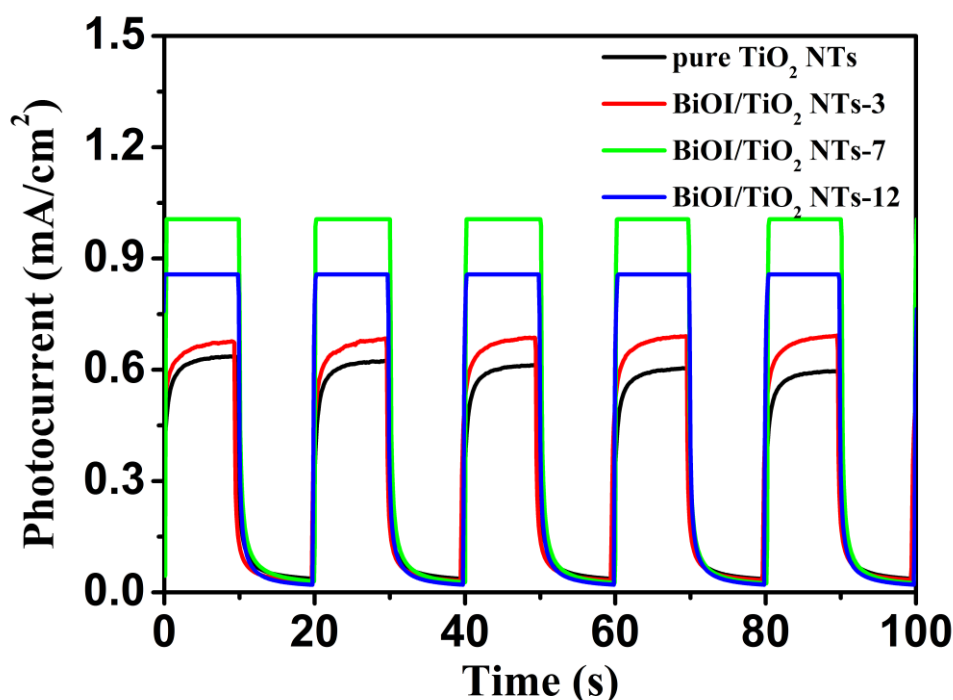
Figure 3. Transient photocurrent responses of samples.

Fig. 4(a) shows that the UV–vis absorption spectra of the pure three-dimensional porous TiO_2 NTs and the $BiOI/TiO_2$ NTs-7 samples. In Fig. 4(a), the pure three-dimensional porous TiO_2 NTs had high absorption in the UV region but lower absorption in visible light region. Compared with absorption of TiO_2 NTs, the three-dimensional porous $BiOI/TiO_2$ NTs heterojunction show a significant enhancement in the visible light region. The optical absorption edge red-shift along with the deposition of BiOI, which indicated that the BiOI addition led to absorption increase in visible region. Obviously, the three-dimensional porous $BiOI/TiO_2$ NTs-7 prepared by SILAR method resulted in the shift of the absorbance region toward longer wavelength. Higher visible light absorbance of three-dimensional porous $BiOI/TiO_2$ NTs-7 sample may be due to presence of BiOI in the composites, and make these composites higher photoactive under visible light. It could be seen clearly that the three-dimensional porous $BiOI/TiO_2$ NTs-7 showed the highest efficiency of visible light absorption performance. Therefore, the high visible light response of $BiOI/TiO_2$ NTs-7 exhibited the high visible light absorption, which would be attributed to the foundations for the photoelectric conversion and significantly enhanced photoelectrocatalytic degradation of organic pollutants.

Fig. 4(b) shows band gap value (E_g) of samples. The band gap value (E_g) of a semiconductor can be estimated through the following equation:

$$\alpha h v = A(h v - E_g)^{n/2} \tag{1}$$

where α is the absorption coefficient, h is Planck's constant, v is the frequency of the light, A is proportionality constant, and E_g is band gap. The band gap values of TiO_2 NTs and $BiOI/TiO_2$ NTs-7 are calculated to be 3.12 and 1.78 eV, respectively.

(a)

(a)
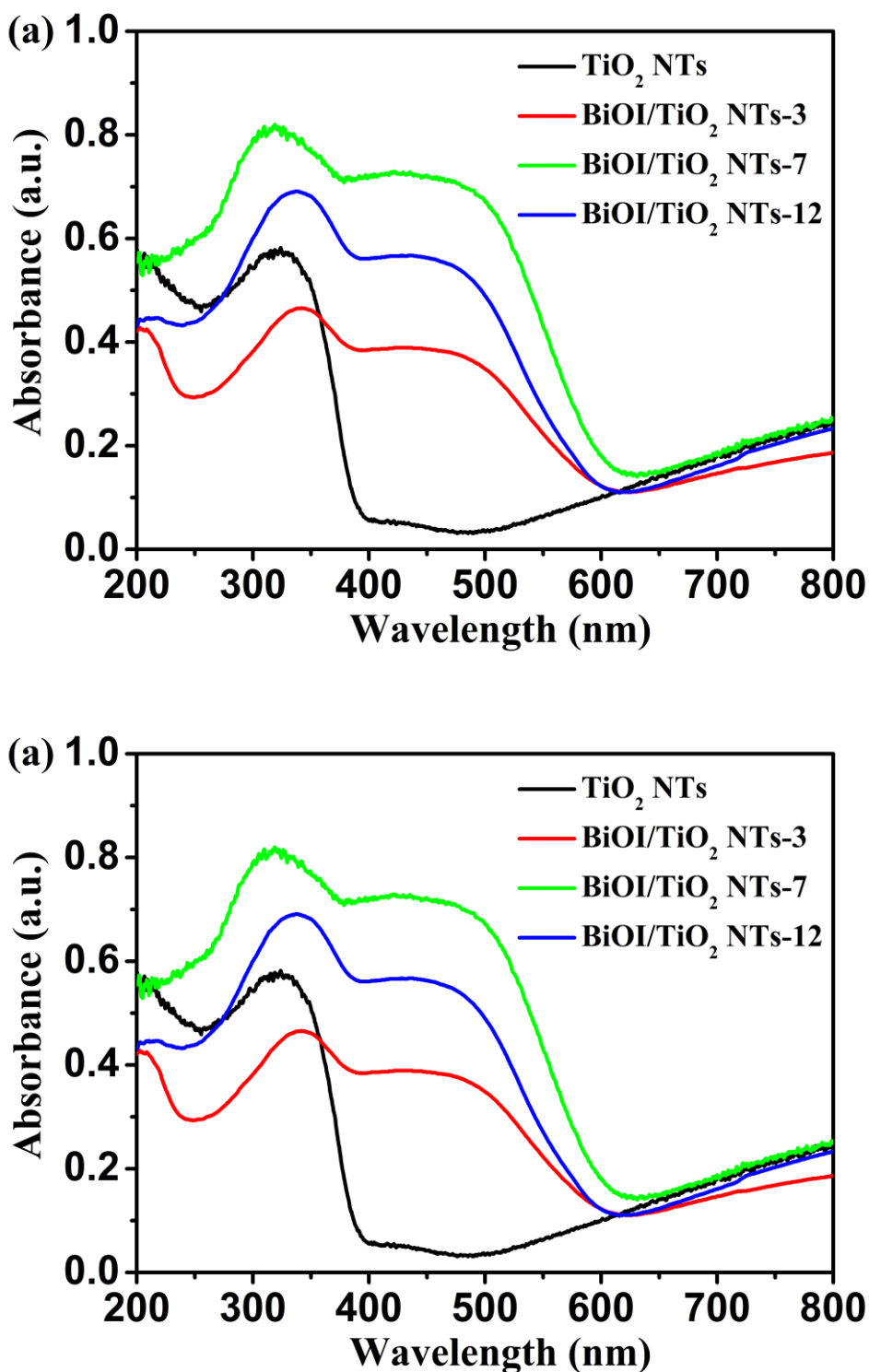
Figure 4. (a) UV-vis diffuse reflectance spectra, (b) band gap energy of samples.

The photocatalytic degradation of RhB by different photocatalysts as a function of time under visible light irradiation was shown in Fig. 5. As was well known, the pure three-dimensional porous TiO_2 NTs presented incapability for RhB degradation, because it almost cannot absorb visible light.

However, the pure BiOI had a narrow band gap so that electro and hole would be recovered quickly upon visible light irradiation. The three-dimensional porous TiO_2 NTs decorated with BiOI nanosheets could overcome these shortcomings. As the samples prepared by SILAR method with the increase of BiOI deposition cycles, and the BiOI/TiO_2 NTs-7 shows the highest photocatalytic activity. As the deposition cycles of BiOI is increased from 7 to 12, a decrease in the photocatalytic activity of BiOI/TiO_2 NTs-12 is observed. This may be since some BiOI nanosheets did not form a heterojunction with TiO_2 NTs, when the BiOI nanosheets were superfluous. The superfluous BiOI nanosheets layer on top of the BiOI/TiO_2 NTs in BiOI/TiO_2 NTs-12 samples, but the BiOI/TiO_2 NTs microstructures could achieve multiple reflections. In the process of visible light irradiation, these pure BiOI nanosheets may act as the recombination centers of photogenerated electrons and holes, leading to a decrease in the photocatalytic activity. Therefore, the high visible light response of BiOI/TiO_2 NTs-7 exhibited the high solar absorption, which would be attributed to the foundations for the photoelectric conversion and significantly enhanced photoelectrocatalytic degradation of organic pollutants.
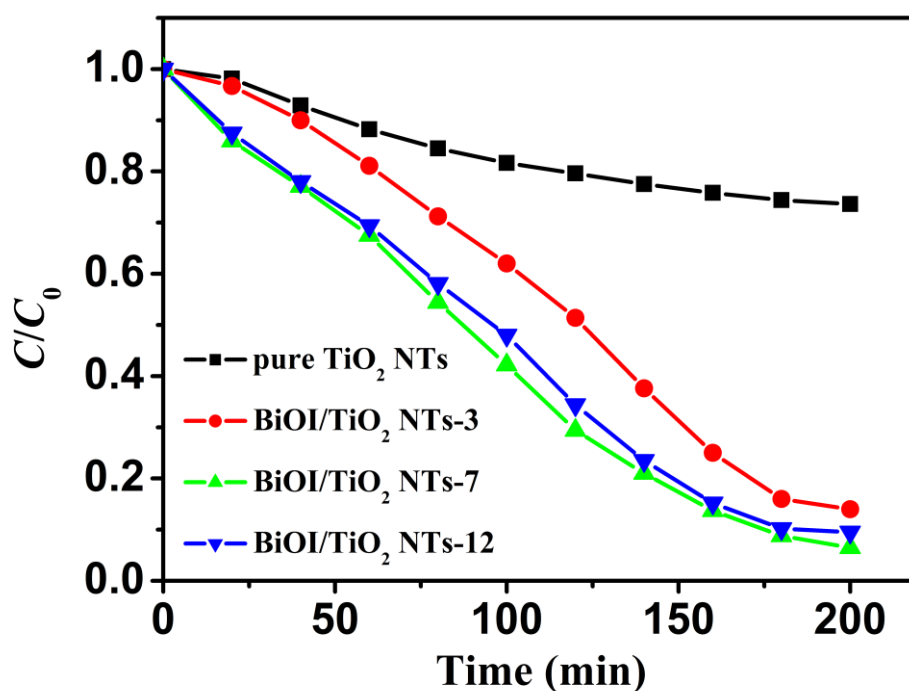
Figure 5. Photocatalytic degradation of RhB with a concentration of 20 mg/L by photocatalyst samples under visible light irradiation.

In particular, BiOI/TiO_2 NTs-7 exhibited the optimal enhanced photoelectrocatalytic degradation of RhB, and the final efficiency reached 93.5% after solar irradiation for 200 min, which reaches to 4 times as much as those of pure TiO_2 NTs. All of BiOI loading samples (BiOI/TiO_2 NTs-3, BiOI/TiO_2 NTs-7, and BiOI/TiO_2 NTs-12) effectively degrade the RhB dye under visible light, and more efficient when used with BiOI/TiO_2 NTs-7. This may be owing to higher visible light absorption by BiOI/TiO_2 NTs-7 sample confirmed by UV–vis absorption spectra measurements (Fig. 4) and additionally decrease of electron-hole recombination in BiOI/TiO_2 NTs heterojunction. Among these samples, BiOI/TiO_2

NTs-7 is found to be very efficient for RhB degradation under visible light. The table 1 shows the photocatalytic Rhodamine B degradation comparison of TiO_2 NTs-based photocatalysts. The p-n heterojunction construction of TiO_2 NTs-based photocatalysts benefited the solar response, photoelectron separation and photocatalytic reaction. The photo-generated holes tend to be transported toward to the TiO_2 NTs to degrade Rhodamine B, while the photogenerated electrons will move to the BiOI surface and taken away by oxygen in the atmosphere. Through this process, the lifetime of photogenerated charges could be prolonged, as well as the separation rate is promoted [48]. On the other hand, the three-dimensional porous $BiOI/TiO_2$ NTs sample has a larger specific surface area and a higher absorption efficiency of visible light. Consequently, the $BiOI/TiO_2$ NTs-7 exhibited the optimal enhanced photoelectrocatalytic degradation of RhB, and the final efficiency reached 93.5% after solar irradiation for 200 mim.

Table 1 The photocatalytic Rhodamine B degradation comparison of TiO_2 NTs-based photocatalysts.

Photocatalyst	Preparation method	Light source	Efficiency	Ref.
TiO_2 NTs/BiOI	successive ionic layer adsorption and reaction	500 W Xe-lamp ($\lambda >$ 400 nm)	62%	[7]
TiO_2 NTs/Bi_2MoO_6	solvothermal method	500 W Xe-lamp ($\lambda >$ 400 nm)	75%	[45]
TiO_2 NTs/CdS–CuS	hydrothermal deposition	300 W Xe-lamp ($\lambda \geq$ 420 nm)	78.86%	[46]
Bi/Bi_2MoO_6/TiO_2 NTs	solvothermal method	500 W Xe-lamp ($\lambda \geq$ 420 nm)	73.21%	[47]
$BiOI/TiO_2$ NTs	successive ionic layer adsorption and reaction	500 W Xe-lamp ($\lambda \geq$ 420 nm)	93.5%	This work

Fig. 6 shows the stability and reusability of the as-prepared $BiOI/TiO_2$ NTs-7 composites for four times. As shown Fig. 6, after four times recycling test for degradation of RhB with $BiOI/TiO_2$ NTs-7 under visible light irradiation, there was only a slight loss in photocatalytic activity as compared to that the fresh $BiOI/TiO_2$ NTs-7 sample. As a result, $BiOI/TiO_2$ NTs-7 can be considered as a highly stable and reusable photocatalyst for the degradation of RhB under visible light irradiation. Consequently, the photocatalytic activity of the $BiOI/TiO_2$ NTs photocatalysts was significantly improved because of the formation of heterojunction and the enhanced visible light absorption.
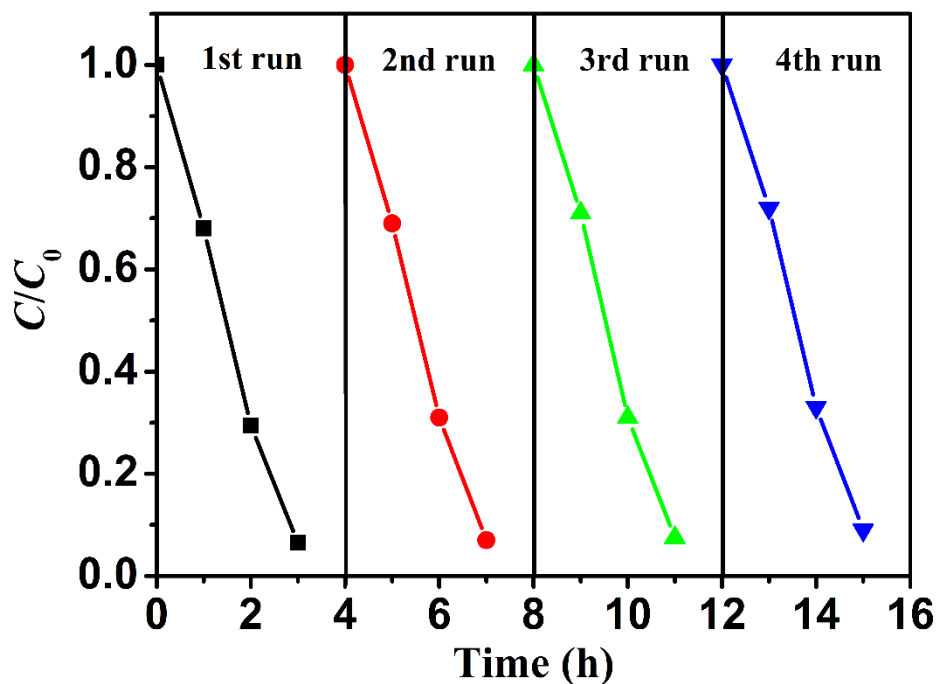
Figure 6. Reusability of BiOI/TiO$_2$ NTs-7 for degradation of RhB for 4 consecutive cycles.

4. CONCLUSIONS

In conclusion, the results from our studies confirmed that the heterostructured three-dimensional porous BiOI/TiO$_2$ NTs photocatalysts presented high photocatalytic activities of RhB degradation. The heterostructured three-dimensional porous BiOI/TiO$_2$ NTs photocatalysts were prepared by anodizing process and the successive ionic layer adsorption and reaction deposition method. When the three-dimensional porous BiOI/TiO$_2$ NTs sample prepared with 7 cycles by SILAR, the catalysts demonstrated enhancing efficiency for photocatalytic degradation of RhB in comparison with pure three-dimensional porous TiO$_2$ NTs. In particular, BiOI/TiO$_2$ NTs-7 exhibited the optimal enhanced photoelectrocatalytic degradation of RhB, and the final efficiency reached 93.5% after solar irradiation for 200 min, which reaches to 4 times as much as those of pure TiO$_2$ NTs. At the same time, BiOI/TiO$_2$ NTs-7 can be considered as a highly stable and reusable photocatalyst for the degradation of RhB under visible light irradiation. The improvement of photocatalytic performance was attributed to the promotion of charge separation and the efficient transfer of photoexcited electron-hole pairs through the formation of heterojunction and enhanced visible light absorbance. The study indicates that the heterostructured BiOI/TiO$_2$ NTs nanocomposite is a promising visible light driven photocatalysts for environmental photocatalysis, photovoltaics, and sensing applications.

References

1. J.W. Fu, J.G. Yu, C.J. Jiang, B. Cheng, *Adv. Energy Mater.*, 8 (2018) 1701503.
2. M.S. Zhu, S. Kim, L. Mao, M. Fujitsuka, J.Y. Zhang, X.C. Wang, T. Majima, *J. Am. Chem. Soc.*, 139 (2017) 13234.
3. Y.H. Zhang, Z.R. Tang, X.Z. Fu, Y.J. Xu, *ACS Nano*, 4 (2010) 7303.
4. Y.Z. Hong, Y.H. Jiang, C.S. Li, W.Q. Fan, X. Yan, M. Yan, W.D. Shi, *Appl. Catal. B-Environ.*, 180 (2016) 663.
5. F. Xu, H. Tan, J. Fan, B. Cheng, J. Yu, J. Xu, *Sol. RRL*, 5 (2021) 2000571.
6. Y. Zhang, F. Zhang, Z. Yang, H. Xue, D.D. Dionysiou, *J. Catal.*, 344 (2016) 692.
7. Z. Liu, Q. Wang, X. Tan, Y. Wang, R. Jin, S. Gao, *Sep. Purif. Technol.*, 215 (2019) 565.
8. P. Mazierski, A. Malankowska, M. Kobylański, M. Diak, M. Kozak, M.J. Winiarski, T. Klimczuk, W. Lisowski, G. Nowaczyk, A. Zaleska-Medynska, *ACS Catal.*, 7 (2017) 2753.
9. R. Malik, V.K. Tomer, N. Joshi, T. Dankwort, L.K. L. Lin, *ACS Appl. Mater. Interfaces*, (2018) 34087.
10. B. Damardji, H. Khalaf, L. Duclaux, B. David, *Appl. Clay Sci.*, 45 (2018) 98.
11. J. Zhang, Y. Cai, X. Hou, H. Zhou, H. Qiao, Q. Wei, *J. Phys. Chem. C*, 122 (2018) 8946.
12. Y. Zhang, S. Park, *J. Solid State Chem.*, 253 (2017) 421.
13. Y.-R. Lv, C.-J. Liu, R.-K. He, X. Li, Y.-H. Xu, *Mater. Res. Bull.*, 117 (2019) 35.
14. X. Su, J. Yang, X. Yu, Y. Zhu, Y. Zhang, *Appl. Surf. Sci.*, 433 (2018) 502.
15. J. Shang, W. Yao, Y. Zhu, N. Wu, *Appl. Catal. A*, 257 (2004) 25.
16. L. Shan, Y. Liu, J. Bi, J. Suriyaprakash, Z. Han, *J. Alloys Compd.*, 721 (2017) 784.
17. M.F. Abdel-Messih, M.A. Ahmed, A. Shebl El-Sayed, *J. Photochem. Photobiol. A*, 260 (2013) 1.
18. Q. Han, R. Wang, B. Xing, T. Zhang, M.S. Khan, D. Wu, Q. Wei, *Biosens. Bioelectron.*, 99 (2018) 493.
19. Y. Arai, K. Tanaka, A. L. Khlaifat, *J. Mol. Catal. A*, 243 (2006) 85.
20. H. Fujii, K. Inata, M. Ohtaki, K. Eguchi, H. Arai, *J. Mater. Sci.*, 36 (2001) 527.
21. G. Marci, V. Augugliaro, C. Martin, L. Palmisano, A.M. Venezia, *J. Phys. Chem. B*, 105 (2001) 1026.
22. L. Ren, D. Zhang, X.Y. Hao, X. Xiao, Y. Jiang, J.Y. Gong, F. Zhang, X. Zhang, Z. Tong, *Mater. Res. Bull.*, 94 (2017) 183.
23. L. Yosefi, M. Haghighi, *Appl. Catal. B*, 220 (2018) 367.
24. H. Liu, Y. Su, H.J. Hu, W.R. Cao, Z. Chen, *Adv. Powder Technol.*, 24 (2013) 683.
25. J.M. Montoya-Zamora, A.M. Cruz, E.L. Cuéllar, *J. Taiwan Chem. Eng.*, 75 (2017) 307.
26. L.Q. Yi, H. Gui, C.S. Xu, *Mater. Res. Bull.*, 102 (2018) 16.
27. J.L. Lu, Q.G. Meng, H.Q. Lv, L.L. Shui, M.L. Jin, Z. Zhang, Z.H. Chen, M.Z. Yuan, X. Wang, J.M. Liu, G.F. Zhou, *J. Alloy. Compd.*, (2018) 167.
28. Q. Yang, J. Huang, J.B. Zhong, J.F. Chen, J.Z. Li, S.Y. Sun, *Curr. Appl. Phys.*, 17 (2017) 1202.
29. C.W. Siao, H.L. Chen, L.W. Chen, J.L. Chang, T.W. Yeh, C.C. Chen, *J. Colloid Interf. Sci.*, 526 (2018) 322.
30. B. Tahir, M. Tahir, *Appl. Surf. Sci.*, 506 (2020) 145034.
31. J. Di, J.X. Xia, M.X. Ji, B. Wang, S. Yin, H. Xu, Z.G. Chen, H.M. Li, *Langmuir*, 32 (2016) 2075.
32. M. Mahjoubian, A.S. Naeemi, M. Sheykhan, *Chemosphere*, 263 (2021) 128182.
33. R.F. Dong, Y. Hu, Y.F. Wu, W. Gao, B.Y. Ren, Q.L. Wang, Y.P. Cai, *J. Am. Chem. Soc.*, 139 (2017) 1722.
34. Y. Hu, D. Li, Y. Zheng, W. Chen, Y.H. He, Y. Shao, X.Z. Fu, G.C. Xiao, *Appl. Catal. B-Environ.*, 104 (2011) 30.
35. M. Tahir, M. Siraj, B. Tahir, M. Umer, N. Hajar, A. Othman, *Appl. Surf. Sci.*, 503 (2020) 144344.
36. M. Zalfani, B. van der Schueren, Z.Y. Hu, J.C. Rooke, R. Bourguiga, M. Wu, Y. Li, G. Van Tendeloo, B.L. Su, *J. Mater. Chem. A Mater. Energy Sustain.*, 3 (2015) 21244.

37. H. Li, H. Yu, X. Quan, S. Chen, H.M. Zhao, *Adv. Funct. Mater.*, 25 (2015) 3074.
38. N.T. Padmanabhan, N. Thomas, J. Louis, D.T. Mathew, P. Ganguly, H. John, S.C. Pillai, *Chemosphere*, 271 (2021) 129506.
39. G. Odling, N. Robertson, *ChemPhysChem*, 17 (2016) 2872.
40. P. Parnicka, W. Lisowski, T. Klimczuk, J. Łuczak, A. Zak, A. Zaleska-Medynska, *Appl. Catal. B Environ.*, 291 (2021) 120056.
41. M.F.R. Samsudin, S. Sufian, N.M. Mohamed, R. Bashiri, F. Wolfe, R.M. Ramli, *Mater. Lett.*, 211 (2018) 13.
42. Z.Y. Liu, Q.Y. Wang, W.Q. Rong, R.C. Jin, Y.M. Cui, S.M. Gao, *Sep. Purif. Technol.*, 200 (2018) 191.
43. G.P. Dai, J.G. Yu, G. Liu, *J. Phys. Chem. C*, 115 (2011) 7339.
44. J.Q. Liu, L.L. Ruan, S.B. Adeloju, Y.C. Wu, *Dalton Trans.*, 43 (2014) 1706.
45. Z. Liu, Y. Song, Q. Wang, Y. Jia, X. Tan, X. Du, S. Gao, *J. Colloid Interface Sci.*, 556 (2019) 92.
46. J. Hou, B. Huang, L. Kong, Y. Xie, Y. Liu, M. Chen, Q. Wang, *Ceram. Int.*, 47 (2021) 30860.
47. D. Cao, Q. Wang, Y. Wu, S. Zhu, Y. Jia, R. Wang, *Separ. Purif. Technol.*, 250 (2020) 117132.
48. Q. Shi, M. Zhang, Z. Zhang, Y. Li, Y. Qu, Z.Liu, J. Yang, M. Xie, W, Han, *Nano Energy*, 69 (2020) 104448